A time efficient optical model for GATE simulation of a LYSO scintillation matrix used in PET applications

Daniel A B Bonifacio, Nicola Belcari, Sascha Moehrs, Mauricio Moralles, Valeria Rosso, Sara Vecchio and Alberto Del Guerra, *Senior Member, IEEE*

***Abstract*–The dual planar head DoPET (Dosimetry with a Positron Emission Tomograph) tomograph was simulated using GATE (Geant4 Application for Emission Tomography) to evaluate the DoPET performance and its agreement with simulation results including all the relevant physical aspects. An optical model was proposed to predict with accuracy the asymmetrical deterioration of the energy resolution of the detector and at the same time to avoid a too long computation time when activating the optical processes in GATE. The proposed optical model was shown to be around three orders of magnitude faster than a DoPET simulation with GATE optical processes enabled. A good agreement was found between experimental and simulated data using the optical model. This points out that optical interactions inside the crystal elements induce a predictable degradation of the spectra information as acquired by DoPET. Finally, our proposed optical model could be useful to simulate a scintillation matrix and its read out by a position sensitive photomultiplier commonly employed in PET detectors.**

I. Introduction

MONTE Carlo simulation is a very useful tool for the assessment of the performance of medical imaging devices in emission tomography, for the optimization of acquisition protocols, and for the development of image reconstruction algorithms and correction techniques [1]. We are performing a Monte Carlo simulation of the DoPET (Dosimetry with a Positron Emission Tomograph) tomograph [2], which is based on a detector module made of a LYSO scintillation matrix seen by a position sensitive photomultiplier. The GATE (Geant4 Application for Emission Tomography) [3] simulation code for tomographic applications, based on Geant4 toolkit [4], was selected for that task. GATE is a very well diffused tool that features description of time-dependent processes, acquisition and signal processing stage for a complete system simulation.

DoPET features a channel-to-energy calibration procedure that uses as energy reference the 511 keV peak from a ^{22}Na source and also considers that the number of collected optical photons by the photomultiplier (PMT) is proportional to the deposited gamma energy. The light attenuation inside the crystal, which depends on the position of the interaction of the photon and occurs during the light transport before being collected by the PMT, deteriorates asymmetrically the energy resolution of the detector and cannot be taken into account for absolute calibration purposes because of the single side PMT readout scheme.

An evident example of the blurring of the energy resolution of DoPET is the energy spectrum, acquired in single mode, of the ^{176}Lu intrinsic radioactivity present in LYSO crystal. The abundance of ^{176}Lu in the lutetium is about 2.6% and it has a half-life of 3.78 x 10^{10} years. Consequently, the background count rate registered over an acquisition in single mode is approximately 240 cps/cm^3 [5]. According to the ^{176}Lu decay scheme (Fig. 1), the expected maximum energy value in the measured spectrum is around 1.2 MeV. If one naively uses the experimental 511 keV peak of a ^{22}Na source to calibrate linearly the spectrum, a long tail with maximum energy of approximately 1.8 MeV is observed, as can be seen in Fig. 2.

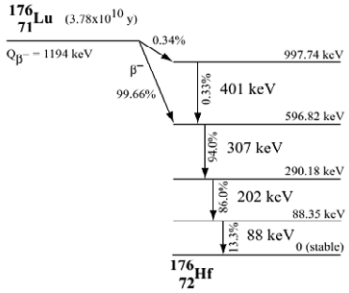

Fig. 1. ^{176}Lu decay scheme to ^{176}Hf [6]. In 99.66% of the cases, ^{176}Lu decays into ^{176}Hf by beta-emission at 597 keV, followed by a cascade of gamma photons with energies of 307, 202 and 88 keV.

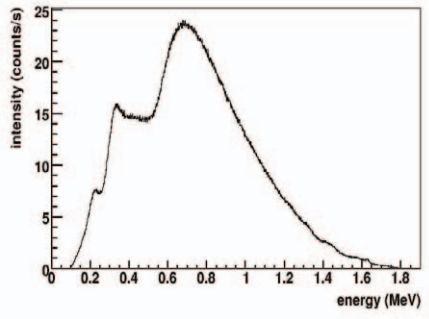

Fig. 2. Spectrum of the ^{176}Lu intrinsic radioactivity measured by the DoPET detector matrix. The energy scale is based on the assumption that the energy released by the 511 keV photopeak is completely collected by the photomultiplier.

Manuscript received November 4, 2009. This work was supported by the Brazilian agencies CNPq and CAPES.

D. A. B. Bonifacio is with the Institute of Physics – University of Sao Paulo, Nuclear and Energy Research Institute -Ipen/CNEN/SP - Brazil and the Department of Physics "E. Fermi", University of Pisa, Italy (email: daniel@if.usp.br)

N. Belcari, V. Rosso, S. Vecchio and Alberto Del Guerra are with the Department of Physics "E. Fermi", University of Pisa, Italy and the INFN Pisa, Italy.

S. Moehrs is with the Department of Physics "E. Fermi", University of Pisa, Italy.

M. Moralles is with the Nuclear and Energy Research Institute - Ipen/CNEN/SP – Brazil.

Thus, the transport of optical photons was included in our simulation with the purpose to reproduce the measured results. However, activating optical processes in GATE makes the simulation about three orders of magnitude slower, becoming highly time consuming. To avoid a too long computation time, an alternative optical model was used to describe the behavior of the optical photons collection by the photomultiplier depending on the DOI (Depth Of Interaction) inside the crystal.

II. Material and Methods

A. DoPET Design

The DoPET tomograph (Fig. 3) consists of two planar heads, each one composed of one array of 21 x 21 optically isolated LYSO ($Lu_{2(1-x)}Y_{2x}SiO_5$, $x \approx 0.1$) crystal elements from Hilger Crystals Ltd (UK), a Hamamatsu H8500C flat panel photomultiplier (PMT) and associated electronics for signal amplification and digitization. Each LYSO element is 2 mm x 2 mm x 18 mm with both end faces polished. Each array is constructed using white epoxy as the reflector material with 0.15 mm of separator thickness. One of the faces is covered by three layers of a 0.08 mm thick PTFE reflector tape (Saint Gobain BC-642) and the other face is optically coupled to a photomultiplier (PMT) using a mounting media (Cargille Meltmount* 1.582). The H8500C PMT has an active area of 49 mm x 49 mm, 8 x 8 channels multi-anode, bialkali photocathode and borosilicate window. The number of acquired signals is reduced from 64 to 4 signals per head by means of a multiplexed read-out[7].

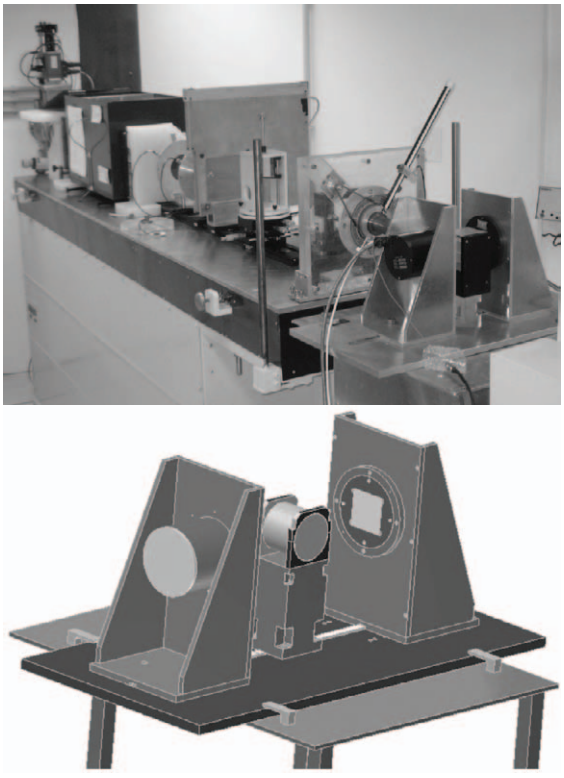

Fig. 3. Photo and schematic view of DoPET. The two planar detector heads and the plastic cylindrical phantom are held by an alluminum-alloy support.[2]

B. Proposed optical model overview

The first step consists of a simplified simulation of a single crystal element of DoPET to obtain the optical attenuation as a function of the distance to the PMT. After that, the model can be employed to calculate the influence of the optical processes in the energy response of the complete crystal matrix present in the tomograph. All the simulations were performed using GATE version 4.0.0, which is based on Geant4 version 9.1.p02.

The model is based on the fit of an analytical function of a second order exponential decay expression:

$$N_{ph}(z) = A\exp(-z/\lambda_1) + B\exp(z/\lambda_2) \qquad (1)$$

Where "N_{ph}" is the number of optical photons that are collected by the PMT after the total energy deposition of a 511 keV photon at a specific depth of interaction "z" in the crystal. The parameters "A", "B", "λ_1" and "λ_2" are the coefficients of the function.

The input data are the mean values of the number of detected optical photons for a specific set of DOI positions, from 0.5 mm to 17.5 mm by 1 mm step. They are obtained from a simplified simulation with the optical processes activated, which consists of 511 keV photons interacting and depositing all their energy at the center of a single crystal element along its longitudinal axis. The simulation is illustrated in Fig. 4, which also shows the relevant materials and their optical couplings.

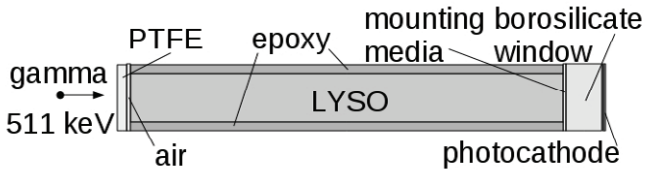

Fig. 4. Simplified scheme of the simulated optical layers, volumes and materials used in GATE.

If one assumes that the light yield is the same for all values of deposited energy by the gamma photons, it is possible to use (1) to obtain the number of optical photons for any value of deposited energy inside the crystal according to the DOI.

Thus, the complete simulation for the DoPET detector was performed using all the relevant processes, except the time consuming optical processes, and (1) was applied on the energy value originated from the "Hits" data output to model the behavior of optical photons interactions inside each crystal element:

$$E_{reg} = E_{dep}(N_{ph}(z)/N_{ph511}) \qquad (2)$$

Where E_{reg} is the registered energy by the detector after calibration procedure, E_{dep} is the deposited energy and N_{ph511} is the number of photons corresponding to the 511 keV peak used in the energy calibration.

1) Simplified simulation aspects: optical processes active

To find the fitting parameters of (1), a simulation with the following simplifications was used. With respect to the physical processes involving gamma interactions, only photoelectric effect from the Standard physical model was activated in GATE, while Compton and Rayleigh scattering

remained inactive. The electron cut was set to avoid secondary electron production. Thus, for each interaction occurring inside the crystal all the gamma energy is deposited at once in a specific region and the number of optical photons generated are related to the incident 511 keV gamma.

While scintillation is responsible for the optical photon production, the physical processes concerning optical photon interactions are optical absorption, optical Rayleigh scattering, as well as refraction and reflection on the interaction between surfaces. These processes require the definition of some specific material properties.

LYSO properties comprise light yield (32 photons/keV), time decay constant (41 ns), absorption length (50 cm), Rayleigh scattering length (260 cm) and emission peak wavelength (420 nm). The index of refraction was set as a function of the optical photon wavelength [8].

White epoxy, PTFE tape, mounting media and borosilicate window were assumed to have an index of refraction of 1.53, 1.34, 1.582 and 1.51, respectively.

It is known that self-absorption is usually not a significant loss mechanism [9]. However, interactions between surfaces play an important role in the present simulations. Geant4 provides two implementations of optical boundary process: GLISUR and UNIFIED models[10], but only UNIFIED model can be used under the GATE framework. UNIFIED model simulates optical interactions only between two dielectric media[11]. Thus, to properly obtain the fitting data at 511 keV, the "GateSurface" class was changed to permit also the use of the GLISUR optical model, which is the recommended one to simulate a dielectric_metal surface using the complex index of refraction of a metal, like the bialkali photo-cathode of a PMT.

Table 1 shows the properties adopted for the surface between LYSO crystal and epoxy layer and the surface between LYSO crystal and PTFE tape. σ_α is the standard deviation of the normal distribution of angles α which are sampled to define the roughness of a surface with micro-facets whereas each one has a normal vector which deviates from the mean normal by an angle α. N_I is the index of refraction of the intermediate layer between the surfaces. The probabilities occurrence for the different reflection mechanisms provided by the UNIFIED model are defined by four constants. C_{SL} stands for specular lobe constant and illustrates the probability of specular reflection about the normal of a micro facet. C_{SS} means specular spike constant and represents the specular reflection probability about the average surface normal. C_{BS} is the back scatter constant which sets the probability of backward reflection and has more influence on very rough surfaces. The diffuse lobe constant is implicit and represents the probability of internal Lambertian reflection. The sum of the four constants must be one.

The surface type dielectric_metal and finish polished from GLISUR model were employed in the surface between PMT window and its photo-cathode which has a complex index of refraction [12] and quantum efficiency reported in [13]. Moreover, all other surfaces were assumed to have properties commonly used in a dielectric/dielectric smooth surface: UNIFIED model, ground finish, σ_α = 0.1 degrees and specular lobe constant 1.

TABLE 1. PROPERTIES FOR LYSO-PTFE AND LYSO-EPOXY SURFACES

Name	LYSO-PTFE	LYSO-Epoxy
model	UNIFIED	UNIFIED
type	dielectric_dielectric	dielectric_dielectric
finish	groundbackpainted	groundbackpainted
σ_α	0.1 degrees	4.0 degrees
N_I	1.0 (air)	1.53 (epoxy)
C_{SL}	1	1
C_{SS}	0	0
C_{BS}	0	0
reflectivity	0.98	0.94
efficiency	0	0

2) Complete simulation aspects: applying the optical model

The selected physical processes for the complete DoPET simulation were photoelectric effect and Compton and Rayleigh scattering from the Low Energy physical model. The optical model presented in the previous section was employed instead of activating the optical processes simulation. Currently, the readout module of GATE regroups the pulse per block by selecting the position of the pulse of maximum energy. Thus, the "GateReadout" class was modified to calculate the position of the pulse based on a PMT using the resistive chain configuration. The energetic resolution at 511 keV was set to 15.4% (FWHM) as measured experimentally and a coincidence window of 10 ns was used. Finally, the distance between the two detector heads was kept at 14 cm.

We performed simulations with and without the use of the optical model to be compared with the experimental results from the DoPET tomograph. The particle-emitting isotopes were simulated using the General Particle Source (GPS) module [14] provided by Geant4. One simulation consisted of an acquisition of the ^{176}Lu intrinsic radioactivity present in the LYSO crystal and was performed filling the crystal volume with an uniform distribution of ^{176}Lu defined using the GPS module. The other simulation took into consideration the same LYSO background activity and also specifies with GPS a ^{22}Na point-like source placed at the center of the field of view of the tomograph.

III. RESULTS

Figure 5 shows the relation between the mean number of optical photons detected by the PMT and the position of the deposited gamma energy inside a single crystal, calculated with the methodology described in section II.B. The fitted function (1) has the following parameters: A=851 photons, λ_1=4.31 mm, B=491 photons, λ_2=100.00 mm. The light collection efficiency decreases with the distance of the interaction point to the PMT. At the extremity of the crystal its value falls to less than half of the intensity calculated at the nearest point from the PMT.

The energy deposition of the 511 keV photons occurs with the highest probability in the frontal region of each crystal element, which is more distant from the PMT. For calibration purposes, it was assumed that the number of optical photons

corresponding to the position at that extremity of the crystal element (18 mm) is the one associated with the 511 keV peak (N_{ph511}=600.98 photons).

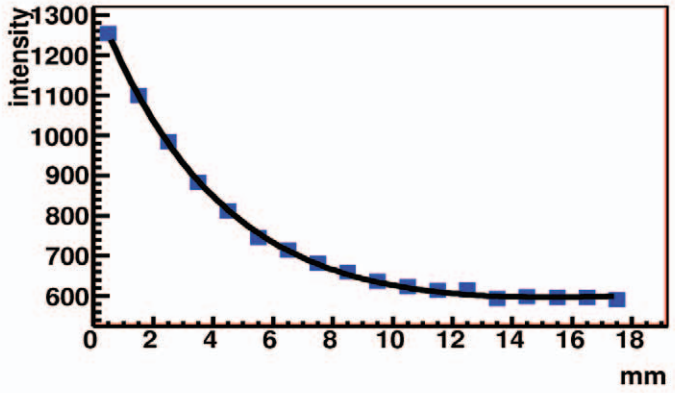

Fig. 5. Mean number of optical photons detected by the PMT according to the position of the deposited gamma energy inside a single crystal.

Fig. 6 and Fig. 7 show the simulated and measured spectra of the DoPET acquisition of LYSO intrinsic radioactivity taken in single and coincidence modes, respectively. Since the density of ^{176}Lu inside the crystal can be calculated using the density of natural Lu present in the LYSO crystal, the intensities are presented as absolute values and are given in counts/s.

Fig. 6 shows the measured and simulated spectra of LYSO intrinsic radioactivity acquired in single mode. The simulated spectrum that uses the optical model (Fig. 6b) presents a much better agreement with the measured spectrum. The differences between both simulated spectra show that the degradation of the energy resolution is due to the optical photon attenuation along the crystal. This effect is easily noticeable at the 202 and 307 keV peaks. In the long tail formed in the high energy part of the spectrum, we see that gamma energy deposited near the PMT implies a higher collection of optical photons when compared with the same amount of gamma energy deposited in a more distant position from the PMT. The use of the Geant4 Low Energy package permits to see the 88 keV peak, which is due to atomic deexcitation. This peak is suppressed in the measured spectrum due to threshold settings applied in the associated electronics to avoid electronic noise.

Fig. 7 exhibits the measured and simulated spectra of LYSO intrinsic radioactivity acquired in coincidence mode. The coincidence events occur due to the detection of the beta-minus particle in one of the heads and the detection of at least one the subsequent gamma photons in the other head. With the exception of the suppressed peak of 88 keV, all the other peaks are present. Concerning the intensity of the peaks, the 307 keV peak of the simulated spectrum without optical model (Fig. 7a) is higher than the measured one. The agreement is much better with the inclusion of the optical model (Fig. 7b).

The count rates obtained for the full spectra are also in a good agreement, as can be seen in Table 2. The count rates values represent only the background noise. Dead time and pile up losses are negligible in this situation of data acquisition at low count rates.

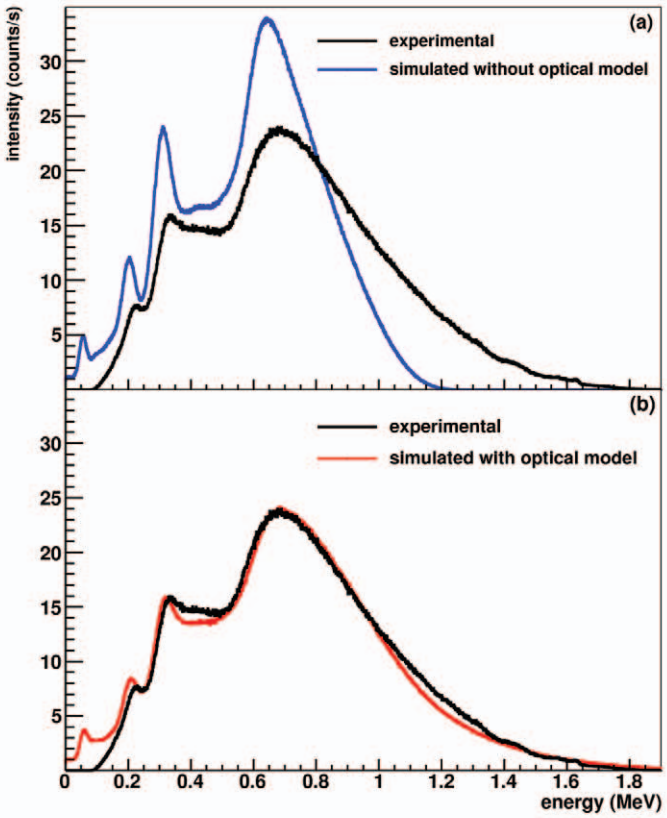

Fig. 6. Comparison of the simulated DoPET spectra without (a) and with (b) the use of the optical model, with the measured spectrum of the LYSO crystal intrinsic radioactivity (^{176}Lu) acquired in single mode.

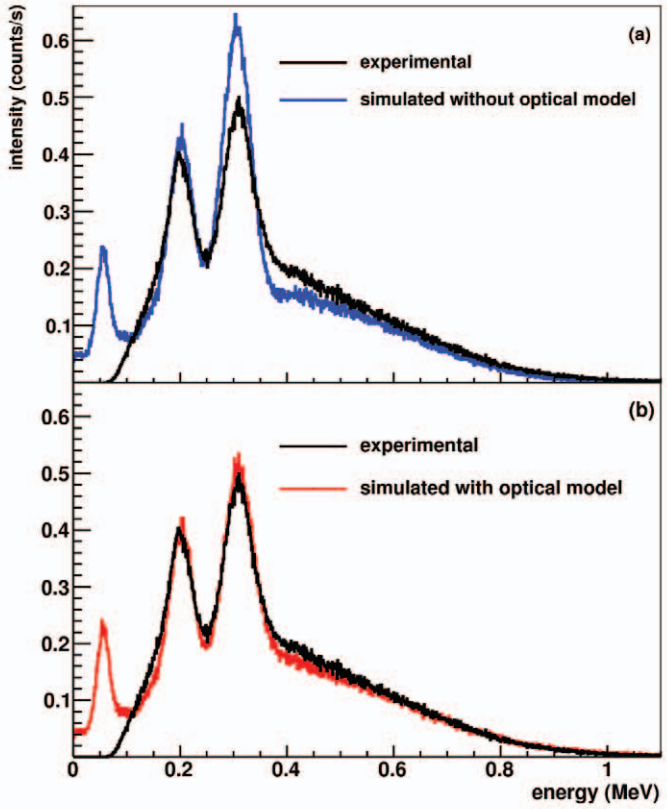

Fig. 7. Comparison of the simulated DoPET spectra without (a) and with (b) the use of the optical model, with the measured spectrum of the LYSO crystal intrinsic radioactivity (^{176}Lu) acquired in coincidence mode.

TABLE 2. COUNT RATES OBTAINED WITH SIMULATED AND MEASURED RESULTS OF THE LYSO CRYSTAL INTRINSIC RADIOACTIVITY.

	count rates (cps)	
	singles	coincidences
experimental	16883	65.1
simulated	16820	63.2

The measured and simulated spectra of a ^{22}Na point-like source at the centre of the field of view and acquired in single mode are shown in Fig. 8. In this situation, the activity value of the ^{22}Na source used in the experiment is not precise, presenting a uncertainty of 30%. Therefore, the spectra is normalized by the area and the intensity, given in counts/s, is arbitrary.

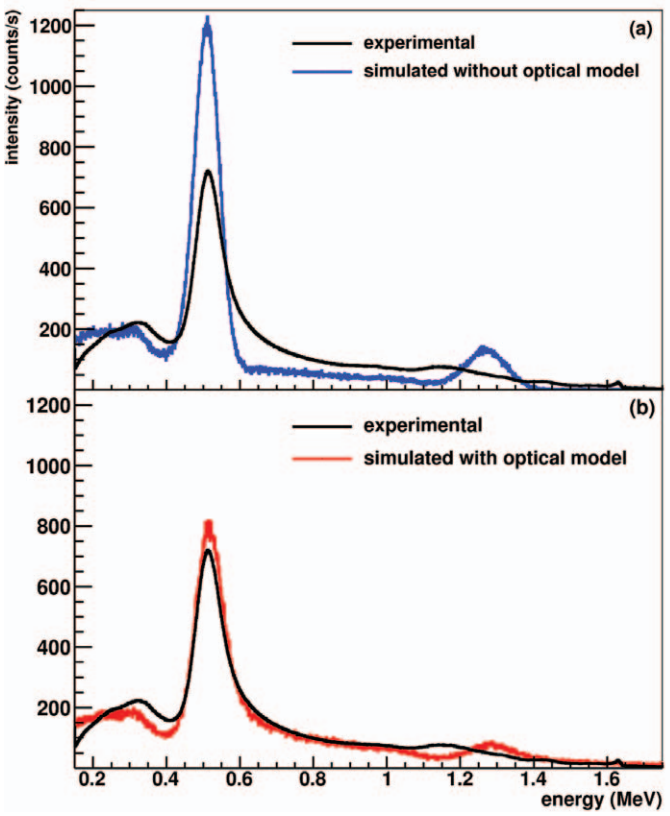

Fig. 8. Comparison of the simulated DoPET spectra without (a) and with (b) the use of the optical model, with the measured spectrum of a ^{22}Na point-like source located in the center of the field of view acquired in single mode.

A good agreement was obtained using the optical model (Fig. 8b) to describe the long tail beginning at 511 keV. However, the 1275 keV peak appears in a shifted position that it is not very well described in the present simulation results. The scattering part of the spectra between the energies 150-400 keV also are presented in a slightly different position.

Fig. 9 exhibits the measured and simulated spectra, acquired in coincidence mode, of a ^{22}Na point-like source located in the center of the field of view (FOV) of DoPET. The spectra were obtained with a low energy cut at 150 keV. Again, the simulated spectrum with the proposed optical model (Fig. 9b) has a much better agreement with the experimental spectrum. The long tail present at the end of the experimental spectrum is only reproducible taking into consideration optical interactions in the scintillator.

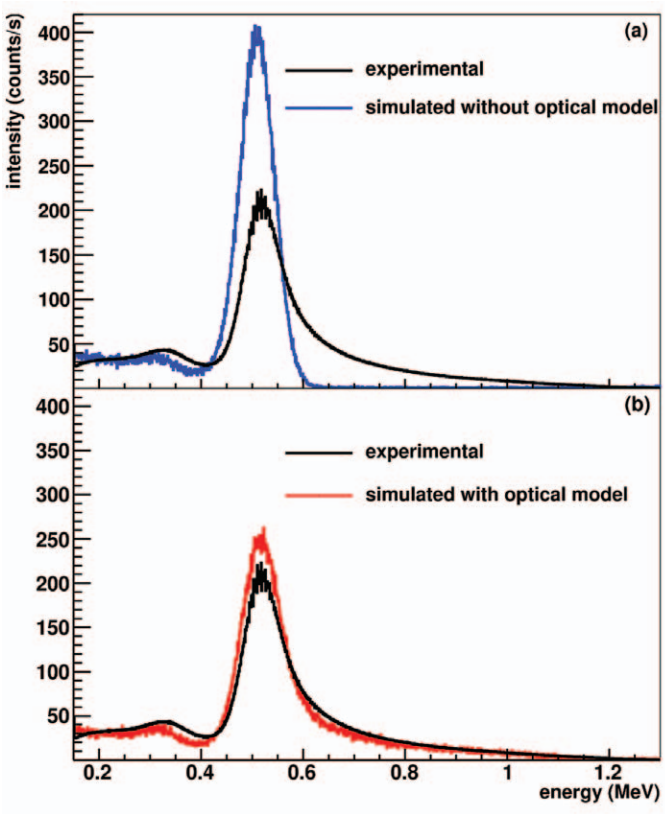

Fig. 9. Comparison of the simulated DoPET spectra without (a) and with (b) the use of the optical model, with the measured spectrum of a ^{22}Na point-like source located in the center of the field of view acquired in coincidence mode.

The optical attenuation along the crystal causes DoPET to loose around 10 % of events during a registration using a 850 keV high energy threshold.

The proposed optical model was shown to use much less computation time when compared to a DoPET simulation with optical processes enabled. In fact, using an AMD Sempron based CPU, a DoPET simulation using a point-like ^{22}Na source and optical processes inactive needed several hours of computation time, whereas to apply (1) on the data output only takes several minutes. On the other hand, a GATE simulation using optical processes would be about 1000 times slower.

IV. DISCUSSION AND CONCLUSION

The dual planar head DoPET tomograph was simulated using GATE to evaluate the DoPET performance and its agreement with simulation results including all the relevant physical aspects for PET applications. A time efficient optical model was proposed to predict with accuracy the simulated energy spectra and to avoid a too long computation time when activating the optical processes in GATE. The use of the proposed optical model was shown to be around three orders of magnitude faster than a DoPET simulation with GATE optical processes enabled.

Simulations without and with modeling of the optical photon attenuation along each LYSO crystal element were

performed. A very good agreement was found between experimental and simulated data with the inclusion of this optical model. This points out that optical interactions inside the crystal elements play an important role on the energy resolution and induce a consequent degradation of the spectra information acquired by the tomograph. The calibration procedure adopted by the DoPET tomograph is appropriate for its clinical applications, but it does not take in consideration the non-linear detector response noticed in Figure 8. Moreover, this work also shows that the commonly used energy thresholds (350-850 keV) applied in DoPET to select the coincidence events leads DoPET to lose around 10% of good coincidence events. Thus, it is possible to improve the system detection efficiency by increasing the high energy threshold.

Finally, our proposed optical model could be useful to simulate a scintillation matrix and its read out by a position sensitive photomultiplier commonly employed in PET detectors. The same model can also be used to simulate others PET/SPECT system based in scintillation pixel matrix using single [15]-[19] or dual readout scheme[20;21].

References

[1] H. Zaidi, "Relevance of accurate Monte Carlo modeling in nuclear medical imaging," Medical Physics, vol. 26, Apr. 1999, pp. 574-608.

[2] S. Vecchio, F. Attanasi, N. Belcari, M. Camarda, G. Cirrone, G. Cuttone, F. Di Rosa, N. Lanconelli, S. Moehrs, V. Rosso, G. Russo, and A. Del Guerra, "A PET Prototype for "In-Beam" Monitoring of Proton Therapy," Nuclear Science, IEEE Transactions on, vol. 56, 2009, pp. 51-56.

[3] S. Janet al, "GATE: a simulation toolkit for PET and SPECT," Physics in Medicine and Biology, vol. 49, 2004, pp. 4543-4561.

[4] S. Agostinelli et al, "Geant4--a simulation toolkit," Nuclear Instruments and Methods in Physics Research Section A: Accelerators, Spectrometers, Detectors and Associated Equipment, vol. 506, Jul. 2003, pp. 250-303.

[5] J.S. Huber, W.W. Moses, W.F. Jones, and C.C. Watson, "Effect of 176Lu background on singles transmission for LSO-based PET cameras," Physics in Medicine and Biology, vol. 47, Oct. 2002, pp. 3535-3541.

[6] P. Rodrigues, A. Trindade, and J. Varela, "Clear-PEM system counting rates: a Monte Carlo study," Journal of Instrumentation, vol. 2, 2007, p. P01004.

[7] N. Belcari, A. Del Guerra, M. Camarda, L. Spontoni, S. Vecchio, and D. Bianchi, "Performance of a four-output front-end electronics for multi-anode PMTS readout of scintillator arrays," Nuclear Instruments and Methods in Physics Research Section A: Accelerators, Spectrometers, Detectors and Associated Equipment, vol. 572, Mar. 2007, pp. 335-337.

[8] R. Mao, Liyuan Zhang, and Ren-Yuan Zhu, "Optical and Scintillation Properties of Inorganic Scintillators in High Energy Physics," Nuclear Science, IEEE Transactions on, vol. 55, 2008, pp. 2425-2431.

[9] G.F. Knoll, "Radiation detection and measurement. 3rd," New York, John, 2000, pp. 247-248.

[10] Geant4 Collaboration, "Geant4 User's Guide for Application Developers," Jun. 2009.

[11] A. Levin and C. Moisan, "A more physical approach to model the surface treatment of scintillation counters and its implementation into DETECT," Nuclear Science Symposium, 1996. Conference Record., 1996 IEEE, 1996, pp. 702-706 vol.2.

[12] D. Motta and S. Schönert, "Optical properties of bialkali photocathodes," Nuclear Instruments and Methods in Physics Research Section A: Accelerators, Spectrometers, Detectors and Associated Equipment, vol. 539, Feb. 2005, pp. 217-235.

[13] Hamamatsu Technical Information, "H8500 PSPMT series," 2009.

[14] J. Allison et al, "Geant4 developments and applications," Nuclear Science, IEEE Transactions on, vol. 53, 2006, pp. 270-278.

[15] R.R. Raylman, S. Majewski, B. Kross, V. Popov, J. Proffitt, M.F. Smith, A.G. Weisenberger, and R. Wojcik, "Development of a dedicated positron emission tomography system for the detection and biopsy of breast cancer," Nuclear Instruments and Methods in Physics Research Section A: Accelerators, Spectrometers, Detectors and Associated Equipment, vol. 569, Dec. 2006, pp. 291-295.

[16] H. Alva-Sánchez, A. Martínez-Dávalos, E. Moreno-Barbosa, B. Hernández-Reyes, T. Murrieta, C. Ruiz-Trejo, M. Brandan, and M. Rodríguez-Villafuerte, "Energy calibration of individual crystals in a LYSO pixelated array for microPET detection modules using Voronoi diagrams," Nuclear Instruments and Methods in Physics Research Section A: Accelerators, Spectrometers, Detectors and Associated Equipment, vol. 596, Nov. 2008, pp. 384-389.

[17] A. Del Guerra, A. Bartoli, N. Belcari, D. Herbert, A. Motta, A. Vaiano, G. Di Domenico, N. Sabba, E. Moretti, G. Zavattini, M. Lazzarotti, L. Sensi, M. Larobina, and L. Uccelli, "Performance evaluation of the fully engineered YAP-(S)PET scanner for small animal imaging," Nuclear Science, IEEE Transactions on, vol. 53, 2006, pp. 1078-1083.

[18] Y. Tai, A. Ruangma, D. Rowland, S. Siegel, D.F. Newport, P.L. Chow, and R. Laforest, "Performance Evaluation of the microPET Focus: A Third-Generation microPET Scanner Dedicated to Animal Imaging," J Nucl Med, vol. 46, Mar. 2005, pp. 455-463.

[19] S. Surti, J. Karp, A. Perkins, R. Freifelder, and G. Muehllehner, "Design evaluation of A-PET: A high sensitivity animal PET camera," Nuclear Science, IEEE Transactions on, vol. 50, 2003, pp. 1357-1363.

[20] M. Abreu, J. Aguiar, F. Almeida, P. Bento, B. Carrico, M. Ferreira, F. Goncalves, C. Leong, F. Lopes, P. Lousa, M. Martins, N. Matela, P. Mendes, R. Moura, J. Nobre, N. Oliveira, C. Ortigao, L. Peralta, R. Pereira, J. Rego, R. Ribeiro, P. Rodrigues, J. Sampaio, A. Santos, L. Silva, P. Sousa, I. Teixeira, A. Trindade, and J. Varela, "Design and evaluation of the clear-PEM scanner for positron emission mammography," Nuclear Science, IEEE Transactions on, vol. 53, 2006, pp. 71-77.

[21] J. Huber, W. Choong, J. Wang, J. Maltz, J. Qi, E. Mandelli, and W. Moses, "Development of the LBNL positron emission mammography camera," Nuclear Science, IEEE Transactions on, vol. 50, 2003, pp. 1650-1653.